Ab initio molecular dynamics study of amorphous $CdTeO_x$ alloys: Structural properties

E. Menéndez-Proupin,[1] P. Giannozzi,[2] J. Peralta,[1] and G. Gutiérrez[1]
[1]*Departamento de Física, Facultad de Ciencias, Universidad de Chile, Las Palmeras 3425, 7800024 Ñuñoa, Santiago, Chile*
[2]*Department of Physics, University of Udine, Via delle Scienze 208, I-33100 Udine, Italy*
and CNR-INFM DEMOCRITOS National Simulation Center, I-34014 Trieste, Italy
(Received 11 March 2008; revised manuscript received 15 November 2008; published 21 January 2009)

The structural short-range order of amorphous compounds with the composition $CdTeO_x$ (a-$CdTeO_x$) is investigated by means of *ab initio* molecular dynamics. The interatomic forces have been calculated using a plane-wave pseudopotential implementation of density-functional theory. Molecular dynamics has been performed in the nearly-microcanonical ensemble using the Berendsen algorithm to keep the systems at the desired temperature. The compounds are characterized using the pair distribution functions, angle distribution functions, coordination numbers, histograms of coordination numbers, and a description of the molecular units of the compounds. According to our simulations, a-CdTeO and a-$CdTeO_2$ are more disordered than a-$CdTeO_{0.2}$ and a-$CdTeO_3$. In a-$CdTeO_{0.2}$, the most abundant clusters are $TeCd_4$, $CdTe_4$, $TeCd_3$, and $CdTe_3O$. In the case of a-CdTeO and a-$CdTeO_2$, having structural units of types similar to those found in crystalline phases of the Cd-Te-O system, they show no predominant type of cluster. This absence of predominant building blocks is a signature of chemical disorder, and it seems that Te and O atoms can be freely exchanged, as well as Cd to a lesser extent. Finally, in a-$CdTeO_3$, the most abundant clusters are CdO_6, CdO_5, TeO_3, and TeO_4.

DOI: 10.1103/PhysRevB.79.014205 PACS number(s): 61.43.Bn

I. INTRODUCTION

The study of semiconductor oxides has great technological importance because they appear as native oxides in uncoated semiconductor surfaces, but also can play a key role in semiconductor devices, as SiO_2 in microelectronics. Technological developments based on other semiconductors need a proper control of their oxides, among a family of compatible materials that function as substrates, contacts, coatings, optical windows, etc. CdTe is well known for its applications in solar cells and γ-ray and x-ray detectors.[1] CdTe/CdS heterojunction solar cells are considered promising candidates for large scale terrestrial power conversion, with efficiencies as high as 16.5%.[2] Native oxides on CdTe surfaces have been studied for almost 3 decades.[3–8] Oxidized CdTe thin films, obtained by rf sputtering, have been extensively studied in the last 15 years.[9–23] These films present a depth profile with nearly homogeneous composition, and have potential applications as coating layers and optical windows with tunable band gap in CdTe-based devices. The composing material, a-$CdTeO_x$, has amorphous structure and is a transparent insulator with an optical gap that can be tuned between 1.5 and 3.4 eV, depending on the oxygen content ($0 < x < 3$). Recently, CdTe oxidized films with the addition of indium, grown by pulsed laser deposition, have been proposed as transparent conducting oxide and transparent oxide semiconductor,[24] opening new potential applications for this family of materials. Another related material, crystalline Cd_3TeO_6, has been predicted to be n-type semiconductor and candidate for transparent conducting oxide.[25,26]

The exploitation of these properties requires understanding the mechanisms that govern the optical and transport properties. This is hampered by lack of information about the atomic arrangement in a-$CdTeO_x$. Most of the experimental work on the amorphous oxidized CdTe thin films up to now has been devoted to the optimization of growth techniques,[9,10,12,13,20] phase identification, element quantification,[11,14] and description of the optical[9,15,17–19] and vibrational properties.[21,22] Employed techniques include optical, Raman, x-ray photoemission, and Auger electron spectroscopy. For a few crystalline phases, diffraction studies[27,28] have been published, but nothing is known about the structure of the amorphous phases.

On the theoretical side, some effort has been devoted to study the electronic properties of the crystalline phases of the binary and ternary compounds of Cd, Te, and O (see Refs. 26, 29, and 30 and references therein). These studies provide keys to the short-range order and the electronic properties of the amorphous phases, assuming that the atomic environments in a-$CdTeO_x$ are the same that are present in the crystalline binaries and ternaries. In this work, we test this assumption and provide a quantitative statistical description of the short-range order. Modern *ab initio* simulation provides powerful tools to study complex compounds and to predict structural properties with reasonable confidence. Good structural models provide a solid foundation for the investigation of other properties. One of such tools is *ab initio* molecular dynamics (AIMD).[31] Since its application to the study of silica glasses in 1995,[32] AIMD has become an effective tool to obtain structural models of amorphous materials. Compared to classical molecular dynamics (MD), AIMD circumvents the difficulty of finding interatomic potentials that can treat simultaneously covalent and ionic bonds, bond breaking, and the changing of atomic environments. To account for these processes is particularly important in simulations of a-$CdTeO_x$. For example, the environment of tellurium atoms can vary from being tetrahedrally coordinated by four cadmiums to being tetracoordinated by four oxygens in a bipyramidal configuration with a lone pair of electrons,[29] and can present, in principle, many different first-neighbor coordination shells mixing oxygens and cadmiums. The AIMD

method has already been used to study disordered binary compounds of this family, such as liquid CdTe,[33] liquid Cd_xTe_{1-x},[34] and liquid and amorphous TeO_2.[30]

In this paper we present structural models for a-$CdTeO_x$, with the compositions $x=0.2$, 1, 2, and 3. This stoichiometry, with equal amounts of Cd and Te, is typical of the thin films grown by rf sputtering.[11,12,14] These structural models,[35] in the form of xyz coordinates of the atoms in a supercell, can be used subsequently to calculate electronic properties and spectra, or as starting points to simulate doped materials.

We summarize here the structural properties of the simplest crystalline binary and ternary CdTeO compounds: CdTe, CdO, TeO_2, $CdTeO_3$, and Cd_3TeO_6. Solid CdTe at normal pressure has zinc-blende structure. There, both Cd and Te atoms are surrounded by four atoms of the other species, located at the vertices of a tetrahedron. The coordination number is retained upon melting, although there is a significant fraction of homogeneous bonds (Cd-Cd and Te-Te) and there are infinite branched chains of Te.[33] CdO has rocksalt structure, with Cd and O being coordinated to six atoms of the other type. TeO_2 is a mixed covalent-ionic insulator, the most abundant phase of which is α-TeO_2 or paratellurite. The structural units of paratellurite are TeO_4 distorted trigonal bipyramids (tbps). In each tbp, a Te atom is surrounded by two O atoms in axial positions, and two O atoms in equatorial positions. The third equatorial position around Te is occupied by a lone pair of electrons. The tbps form a three-dimensional network, interconnected through an equatorial and an axial oxygen. Other tellurium oxides are similar at the short range. In β-TeO_2, the TeO_4 tbps are arranged in a layered structure. γ-TeO_2 can be described in terms of TeO_3 pyramids forming chains. However, it is worth to mention that lattice dynamics calculations suggest that all phases of TeO_2 can be regarded as molecular crystals made of weakly bonded TeO_2 molecules.[30] In the glass (g-TeO_2), there is a mixture of TeO_3 and TeO_4 units interconnected through the O atoms. A significant fraction of these units contain one nonbridging oxygen, i.e., an O atom linked to only one Te. In the crystalline ternary compounds there are only Cd-O and Te-O bonds, but not Cd-Te bonds.[29,36] The structural units of $CdTeO_3$ are distorted TeO_3 trigonal pyramids that are linked to each other by Cd atoms. This arrangement is similar to the one found in tellurite glasses.[37,38] Cd atoms are sixfold coordinated with Cd-O bond lengths in the 2.197–2.476 Å range. The bond angles deviate as much as 31° from the ideal octahedral bond angles of 90° and 180°. O atoms always link one Te atom with one, two, or three Cd atoms, and the average coordination of O atoms is 3. In Cd_3TeO_6, Cd atoms can be coordinated by six O, such as in CdO, or by four O. The first coordination shell of Te atoms is composed of three pairs of O atoms, each pair at a bond-length distance of 1.904, 1.924, and 1.948 Å. These lengths lie in the typical range of paratellurite α-TeO_2 and tellurite glasses. The O atoms occupy three nonequivalent crystallographic positions and are linked to one Te atom and two or three Cd atoms. The two arrangements of one O atom with two Cd atoms and one Te atom are nearly planar. One common feature of the crystalline phases is the absence of homopolar bonds. In the ternary compounds, there are no Cd-Te bonds, and O atoms always bridge one tellurium atom with one, two, or three cadmium atoms. A full description of these structural properties can be found in Ref. 29.

In Sec. II we explain the methods. In Sec. III we present the results. In Sec. IV we present our final comments.

II. METHODS

In order to study amorphous $CdTeO_x$ alloys at an atomic level, we used the AIMD technique. The structural models are obtained using the following sequence for each of the compositions studied. First, we define a cubic simulation box with the number of atoms of Cd, Te, and O in the amount corresponding to the composition $CdTeO_x$. We have chosen numbers of atoms that keep approximately constant the number of valence electrons in the *ab initio* calculations. Hence, the simulation box contain $(CdTeO_{0.2})_{30}$, $(CdTeO)_{24}$, $(CdTeO_2)_{19}$, and $(CdTeO_3)_{16}$. The box sizes for CdTe and $CdTeO_3$ were adjusted to the experimental densities $\rho(CdTe)=5.85$ g/cm^3 and $\rho(CdTeO_3)=6.416$ g/cm^3. The volume of the simulation box for $CdTeO_x$ $(0<x<3)$ was calculated as the sum of atomic volumes, which were estimated using a linear interpolation of the atomic volumes for $x=0$ and $x=3$. Hence, the volume per formula unit of $CdTeO_x$ is given as $V(x)=(1-x/3)V(CdTe)+(x/3)V(CdTeO_3)$. The starting configuration has the atoms located at random nonoverlapping positions. The second step is to run a molecular dynamics, using the Verlet algorithm, rescaling the velocities at every step to keep the temperature fixed at 3000 K, in order to lose correlations with the starting configuration. We made a first run with a volume 50% higher than the experimental one during 0.5 ps, in order to facilitate ion diffusion from the initial configuration. As the initial configuration presents very large forces, a time step of 2.5 fs was used at the beginning. A time step of 5 fs was used throughout the rest of the simulation. The MD was continued with the physical volume for 3–5 ps, depending on the oxygen content. Third, we did MD with velocity rescaling using Berendsen's algorithm[39] to drive the system toward 300 K as slowly as possible. In Berendsen's algorithm, the velocities are rescaled at every step by the factor $\sqrt{1+(T/T_i-1)\Delta t/\tau}$, where T_i and T are the instantaneous and the target temperatures, Δt is the time step, and τ is a relaxation time. We used $\tau=1$ ps to rescale from 3000 to 300 K. This method allows to approach asymptotically to a configuration with the desired temperature. However, when the mean temperature (averaged upon fast oscillations) approached the target temperature, the equilibration proceeded too slowly. At this point, we used a reduced $\tau=0.4$ ps to accelerate equilibration. This has no consequence if the system is well below the melting point, so that the atomic positions are practically frozen. Berendsen's rescaling was applied until the end of the MD with $\tau=1$ ps. At equilibrium the total energy makes small oscillations driven by the temperature fluctuations. For sampling we used the last 6 ps of the MD.

The MD simulations have been made using the PWSCF code of the QUANTUM-ESPRESSO package.[40] The interatomic forces have been calculated using the Hellmann-Feynman theorem on the self-consistent electronic ground state at each time step, found with the Perdew, Burke, and Ernzerhof

(PBE) parametrization[41] of the density-functional theory. The first Brillouin zone has been sampled using only the Γ point. A Gaussian smearing, with a smearing parameter of 0.02 Ry, has been applied to the density of states to avoid convergence problems with metallic configurations. A plane-wave basis set has been used, with kinetic-energy cutoffs of 30 and 180 Ry for the expansion of the wave functions and the charge density, respectively. The electron-ion interaction has been treated in the pseudopotential approximation. We used available[42] pseudopotentials for Cd and O, and generated another one for Te.[43] The Cd pseudopotential is ultrasoft,[44] with reference configuration $[\mathrm{Kr}]4d^{10}5s^25p^0$ (where [Kr] means the frozen core electronic configuration). The Te pseudopotential is norm conserving, with reference configuration $[\mathrm{Pd}]5s^25p^35d^1$ and two, one, and one projectors for the 5*s*, 5*p*, and 5*d* levels, respectively. It was generated using the Rappe-Rabe-Kaxiras-Joannopoulos[45] (RRKJ) method with cutoff radii of 2.4 bohr. These pseudopotentials include scalar relativistic effects in the core electrons. The O pseudopotential is ultrasoft, with reference configuration $[\mathrm{He}]2s^22p^4$, and was generated using a norm-conserving RRKJ pseudopotential as intermediate step.

The choice of different pseudizations is dictated by computational convenience: ultrasoft pseudopotentials for O and Cd allow one to reduce the needed kinetic-energy cutoff, while little would be gained by a ultrasoft Te. No problem arises from usage of different kinds of pseudopotentials in the same system, as long as they are generated for the same exchange-correlation functional. We have verified that these pseudopotentials allow good description of the band diagrams of CdTe and α-TeO_2. Moreover, the unit-cell volumes are reproduced within the accuracy of GGA calculations. The theoretical volumes overestimate the experimental ones as follows: 8% for CdTe, 5% for $CdTeO_3$, 5% for CdO, and 4% for α-TeO_2.

III. RESULTS

The structural properties of the *a*-$CdTeO_x$ compounds were studied by calculating interatomic correlations such as pair distribution function (PDF), coordination numbers, and angular distributions. The PDF $g(r)$ and the partial PDFs between the species i and j, $g_{ij}(r)$, are defined as[46]

$$g(r) = \frac{V}{N^2}\sum_{i,j}^{N} \langle \delta(r - r_{ij})\rangle, \tag{1}$$

$$g_{ij}(r) = \frac{V}{N_i N_j}\sum_{k}^{N_i}\sum_{l}^{N_j} \langle \delta(r - r_{kl})\rangle, \tag{2}$$

where N_i and N_j are the number of atoms of species i and j in volume V, and $\langle\cdots\rangle$ means the statistical average taken over all the MD configurations. The partial PDFs satisfy the sum rule

$$g(r) = \sum_{i,j} c_i c_j g_{ij}(r), \tag{3}$$

where $c_i = N_i/N$ is the elemental fraction for each specie. The probability of finding an atom of species j inside a spherical shell between r and $r+\Delta r$ from an atom of species i is given by $n_j 4\pi r^2 g_{ij}(r)\Delta r$, where $n_j = N_j/V$ is the number density. From the position of the first peaks of the partial PDFs we obtain nearest-neighbor (NN) distances, which can be assigned to bond lengths upon comparison with bond lengths in the crystalline compounds.[29] The average coordination number n_{ij} is obtained by integration around the first peak of the partial PDF, $n_{ij} = 4\pi n_j \int_0^{R_{i-j}} g_{ij}(r) r^2 dr$, where the cutoff radius R_{i-j} is chosen near the position of the minimum after the first peak of $g_{ij}(r)$. n_{ij} is the average number of atoms of species j surrounding an atom of species i. They satisfy the rule $N_i n_{ij} = N_j n_{ji}$. In order to obtain trends in the series $CdTeO_x$ we have chosen the same R_{i-j} for all the compounds, despite the fact that they do not correspond exactly to the minima of the partial PDFs for every compound. The cutoff distances R_{i-j} are used to obtain the angle distribution functions (ADFs), which allows one to describe three-body correlations. The ADF is defined as a histogram constructed for angles *A*-*B*-*C*, where *A*, *B*, and *C* correspond to different atomic species, *B* being the central atom. The procedure consists in building two lists of neighbors of the central atom *B*, one for *A*, and another for *C*. In the list, considered are only atoms within the cutoff distances described above. Hence, the angle is measured for each trio *A*-*B*-*C* and the counter of the corresponding box in the histogram is updated. This procedure is repeated for each MD step for all the combinations *A*-*B*-*C*. In the case $A=C$ one must consider different atoms inside the cutoff and avoid double counting.[47]

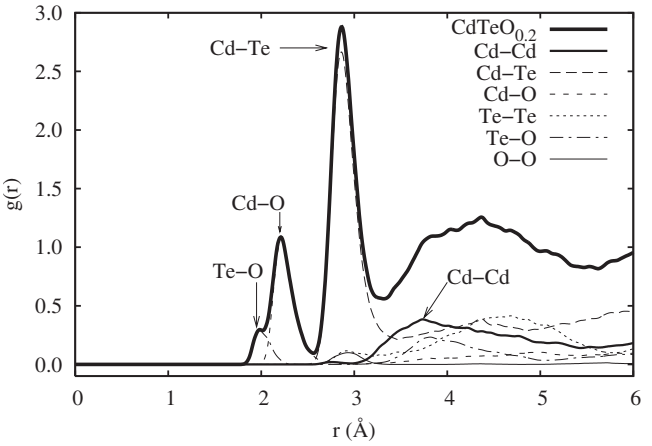

FIG. 1. Total and partial pair distribution functions of *a*-$CdTeO_{0.2}$.

A. Amorphous $CdTeO_{0.2}$

Figure 1 shows the PDF of *a*-$CdTeO_{0.2}$ and the contributions of the partial PDFs $[c_i c_j g_{ij}(r)]$. The PDF has a strong peak for Cd-Te bonds at 2.86 Å, and smaller peaks at 1.96 Å (Te-O bonds) and at 2.20 Å (Cd-O bonds). The partial PDFs reveal a few Te-Te bonds at 2.87 Å. All these distances are close to the bond lengths in crystalline polymorphs. The other peaks in the PDFs correspond to geometrical correlations that are too far to be chemical bonds. For example, the peak at 2.92 Å for O-O corresponds to extreme atoms in O-Te-O and O-Cd-O angles.

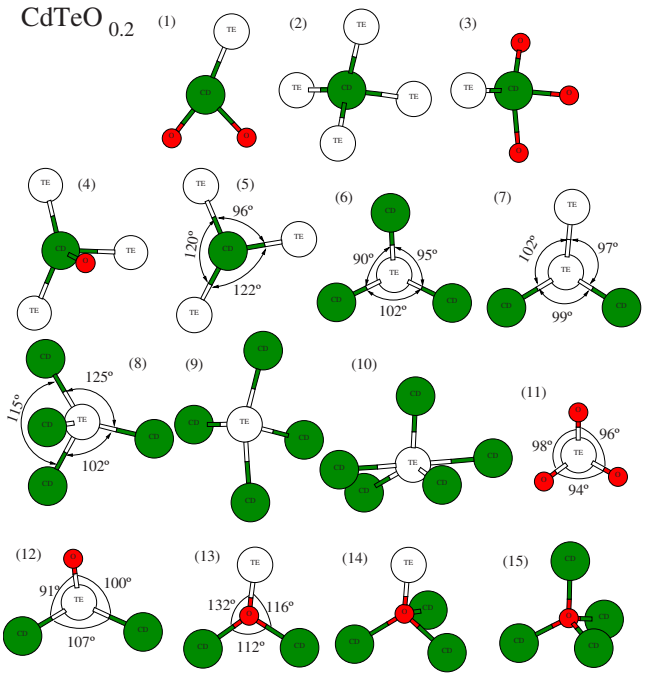

FIG. 2. (Color online) Typical atomic environments in a-$CdTeO_{0.2}$. Filled big spheres, empty spheres, and small spheres correspond to Cd, Te, and O atoms, respectively.

Figure 2 shows the typical atomic environments in a-$CdTeO_{0.2}$. Cd can be coordinated by one Te and two or three oxygens (see cases 1 and 3) such as in crystalline $CdTeO_3$, tetracoordinated by Te such as in CdTe (case 2), three-coordinated by Te in pyramidal form [cluster (5)], and the same shape plus one O [cluster (5)]. Of these clusters, only cluster (1) is nearly planar. Typical Te environments include $TeCd_3$ [cluster (6)], TeO_3 [cluster (11)], Te_2Cd_2 [cluster (7)], and $TeCd_2O$ [cluster (12)] distorted trigonal pyramids, and $TeCd_4$ clusters (8) and (9). Cluster (8) is a distorted tetrahedron with Te at center (see the angles in Fig. 2), and the other [cluster (9)] looks like the trigonal bipyramids found in TeO_2, with O replaced by Cd. Moreover, there is a cluster of Te coordinated by five Cd [cluster (10)]. This cluster has one bond slightly larger than the chosen cutoff distance of 3.19 Å. However, because we have taken average over configurations at 300 K, this fivefold coordinated Te appear in the Te-Cd histogram of Fig. 3. Oxygen appears in three typical environments. One is surrounded by one Te and two Cd [cluster (13)], in a planar configuration, other is a tetrahedral environment with four Cd [cluster (15)] or three Cd and one Te [cluster (14)]. The most abundant clusters are, in this order, $TeCd_4$, $CdTe_4$, $TeCd_3$, and $CdTe_3O$.

The analysis of the partial PDFs suggests that, on average, Cd atoms are surrounded by 3.1 Te atoms and 0.6 O atoms; Te atoms are surrounded by 0.12 O atoms, 3.1 Cd atoms and 0.4 Te atoms, and O atoms are surrounded by 3.1 Cd atoms and 0.6 Te atom. Detailed information about the neighborhood of each atom is provided by a histogram of the distribution of the coordination numbers, as shown in Fig. 3. Cd atoms are mainly coordinated by one to four Te atoms (6%, 16%, 42%, and 35%), and one to three O atoms (in fractions of 35%, 11%, and 2%, respectively). Te atoms are coordinated by one to five Cd atoms (4%, 19%, 38%, 35%, and 2%), one or two Te atoms (27%, 5%), and one to three O atoms (3%, 2%, and 2%). 93% of Te atoms are not connected to O atoms, and 68% are not connected to other Te atoms. O atoms link to two, three, or four Cd atoms (28%, 30%, and 42%) and zero or one Te atom (42% or 58%).

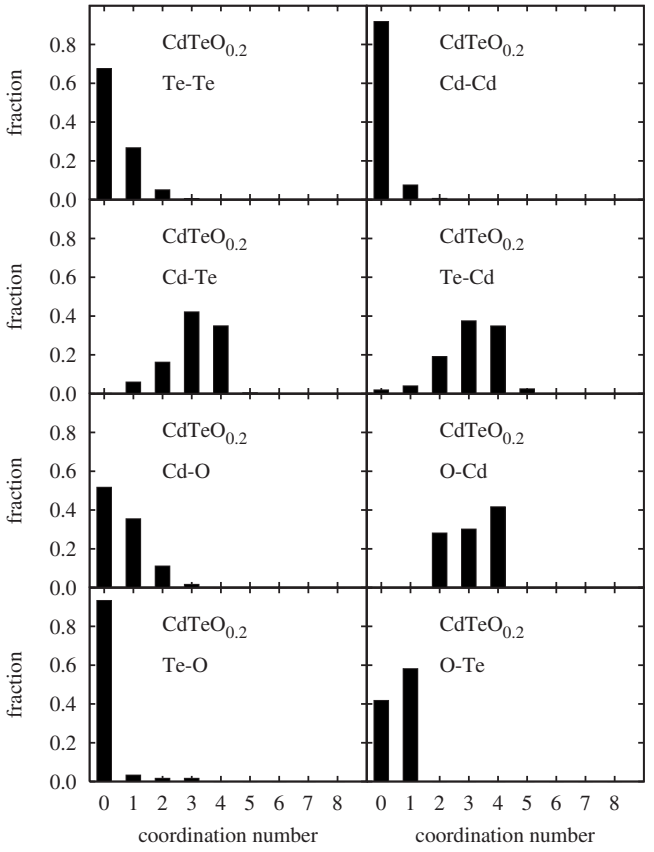

FIG. 3. Histogram of the distribution of the coordination numbers in a-$CdTeO_{0.2}$ computed with cutoff radii of 3.19 Å for Cd-Te and Cd-Cd, 3.27 Å for Te-Te, 2.90 Å for Cd-O, and 2.32 Å for Te-O.

The ADFs of the Cd-O and Te-O bonds are shown in Fig. 4(a). These were computed using the same cutoff distances as the coordination numbers. Angle distributions of Te-Te and Cd-Te bonds are shown in Fig. 4(b). The predominant angles are Cd-Te-Cd, peaked at 90° and Te-Cd-Te with maximum at 106.5°. Less important are the Te-Cd-O and Cd-Te-Te with maxima near 93° and 92°, respectively. Angle O-Te-O has maximum probability at 97°. Angle O-Cd-O probability has maximum at 81°. Angle Cd-O-Cd probability has maxima at 107°, and Cd-Te-O is peaked at 111° and 131°.

B. Amorphous CdTeO

Figure 5 shows the PDF of CdTeO and the contributions of the partial PDFs $[c_i c_j g_{ij}(r)]$. The partial PDFs suggest bonds for Te-O at 1.97 Å, Cd-O bonds at 2.24 Å, Te-Te bonds at 2.83 Å, and Cd-Te bonds at 2.88 Å. All these distances are close to the bond lengths in crystalline polymorphs. When we zoomed the $g_{\text{Te-O}}(r)$ PDF, we found a shoulder

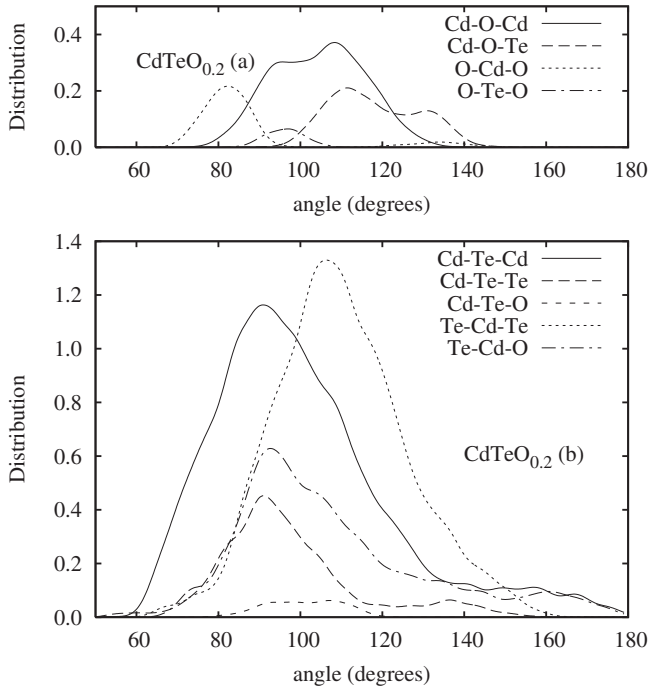

FIG. 4. Angle distribution functions for a-$CdTeO_{0.2}$. In part (a) are the angles involving only Te-O and Cd-O bonds. In part (b) are the angles involving Cd-Te and Te-Te bonds.

at 2.18 Å. Examination of simulation box reveals that this shoulder is related to tellurium-axial-oxygen bonds in bipyramids similar to those that form the structural unit of TeO_2. The other peaks in the PDF correspond to geometrical correlations that are too far to be chemical bonds.

Figure 6 shows the typical atomic environments in a-CdTeO. In cluster (1) there are three O and one Te atoms in the same plane around the central Cd, and one O atom over this plane. Cluster (2) has five atoms in a plane, and one Te over this plane. Clusters (3) and (4) are modifications of cluster (2) eliminating O atoms or replacing by Te. Cluster (5) and (6) are almost planar. In cluster (8), Cd is coordinated by two O and one Te in a planar array, and to other Cd atom at distance 3.08 Å, which is close to the Cd-Cd bond at

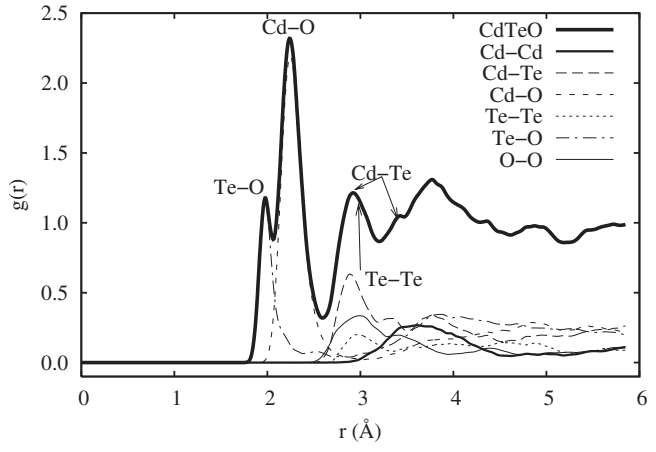

FIG. 5. Total and partial pair distribution functions of a-CdTeO.

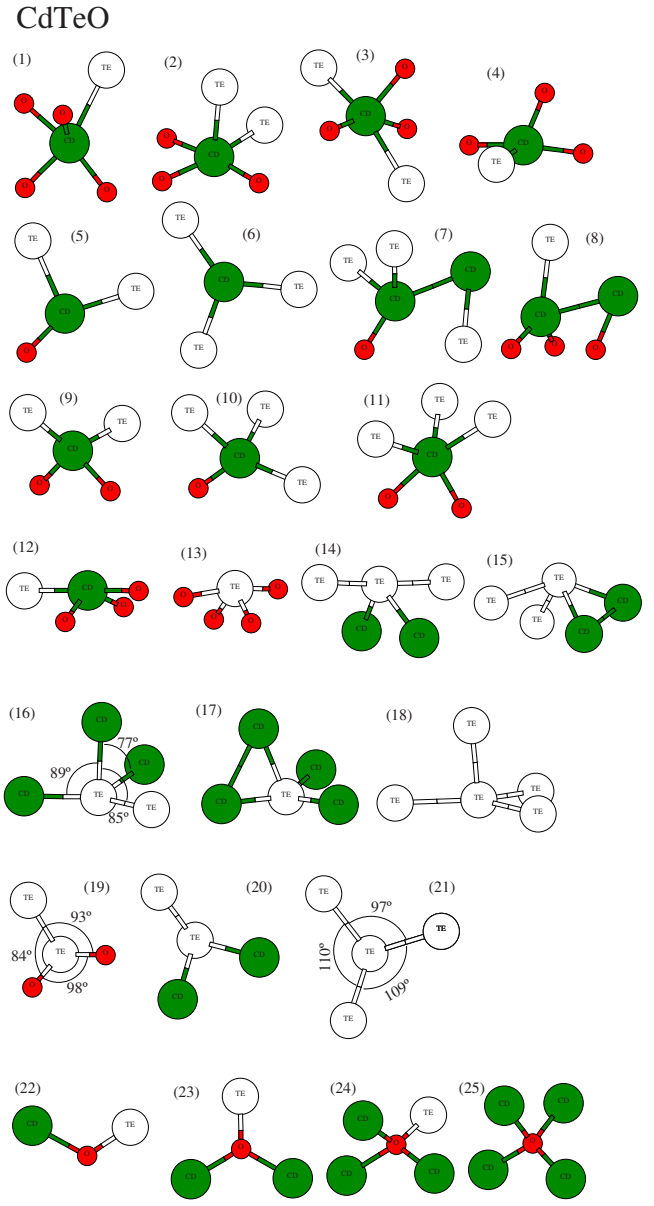

FIG. 6. (Color online) Typical atomic environments in a-CdTeO. Filled big spheres, empty spheres, and small spheres correspond to Cd, Te, and O atoms, respectively.

2.98 Å in elemental Cd. Clusters (9) and (10) form distorted tetrahedra like the basic CdTe units with Cd-Te bonds replaced by Cd-O bonds. Cluster (11) is like the previous ones with the addition of a Te atom. Cluster (7) can be classified with the tetrahedral group, having and additional Te neighbor at 3.15 Å and showing a Cd-Cd bond. Clusters (12)–(15) resemble the TeO_4 bipyramids found in α-TeO_2, but are distorted and have some O atoms replaced by Cd or Te atoms. Clusters (16)–(18) consist of a planar array of triangular shape, with a vertical Cd or Te linked to the central Te. Clusters (19)–(21) are trigonal pyramids with the central Te at the apex, and O, Cd, or Te at the base. Clusters (22)–(25) represent the O environments. Clusters (22) and (23) are planar clusters, while (24) and (25) are tetrahedral clusters. This picture reveals a heavy chemical disorder in CdTeO. Having structural units of similar shapes to those found in crystalline

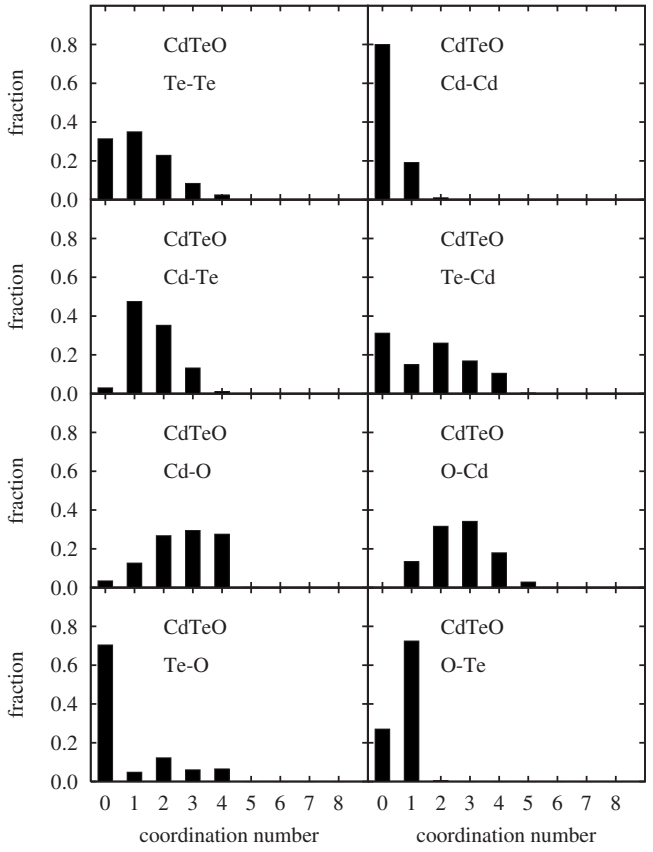

FIG. 7. Histogram of the distribution of the coordination numbers in *a*-CdTeO computed with cutoff radii of 3.19 Å for Cd-Te and Cd-Cd, 3.27 Å for Te-Te, 2.90 Å for Cd-O, and 2.32 Å for Te-O.

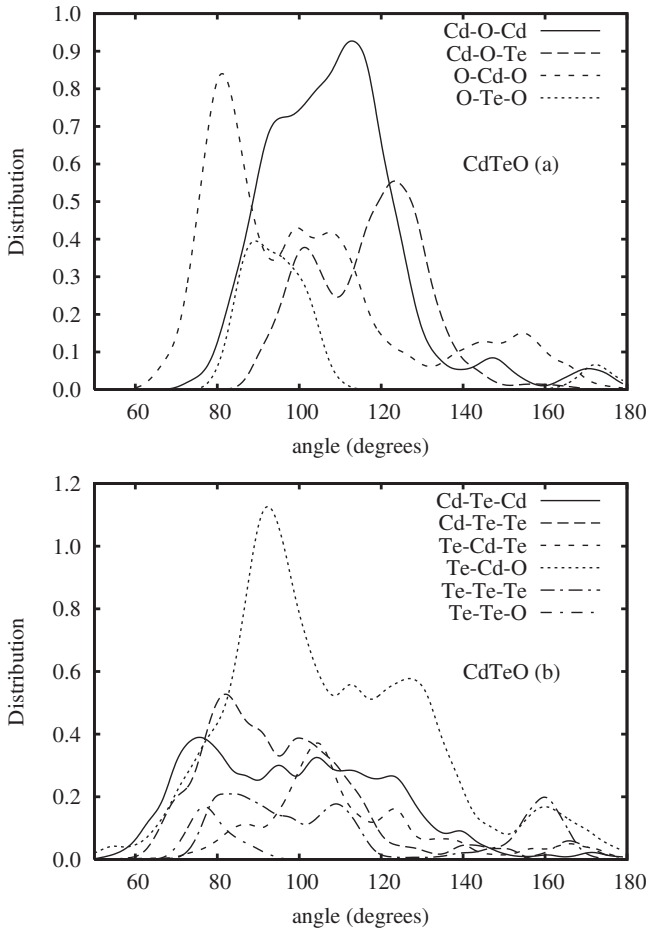

FIG. 8. Angle distribution functions for *a*-CdTeO. In part (a) are the angles involving Te-O and Cd-O bonds. In part (b) are the angles involving Cd-Te and Te-Te bonds.

phases of the Cd-Te-O system, it seems that Te and O atoms can be freely exchanged, as well as Cd in lesser extension, and there is no predominant type of cluster.

The analysis of the partial PDFs suggests that, on average, Cd atoms are surrounded by 2.7 O atoms and 1.6 Te atoms, Te atoms are surrounded by 0.74 O atom, 1.6 Cd atoms, and 1.2 Te atoms, and O atoms are surrounded by 2.6 Cd atoms and 0.74 Te atom. A histogram of the distribution of the Cd-O and Te-O coordination numbers is given in Fig. 7. Cd atoms are mainly coordinated by one to four O atoms (in fractions of 12%, 27%, 30%, and 27%, respectively), and one to three Te atoms (46%, 35%, and 14%). Te atoms are coordinated by one to four Cd atoms (13%, 27%, 16%, and 12%), one to three Te atoms (35%, 22%, and 9%), and one to four O atoms (4%, 12%, 5%, and 7%). 71% of Te atoms are not connected to O atoms, 32% are not connected to Cd atoms, and 31% are not connected to Te atoms. O atoms link to one to four Cd atoms (14%, 31%, 34%, and 17%) and zero or one Te atom (26% and 73%).

The ADFs of the Cd-O and Te-O bonds are shown in Fig. 8(a). These were computed using the same cutoff distances as the coordination numbers. ADFs of Te-Te and Cd-Te bonds are shown in Fig. 8(b). Angle O-Te-O has maximum probability at 92°. Angle O-Cd-O probability is bimodal with peaks at 82° and 107°. Angle Cd-O-Cd probability has maxima at 96° and 106°, and Cd-O-Te is peaked at 102° and 122°. For angles with Te-Cd and Te-Te bonds, the most probable is Te-Cd-O, with a peak at 94° and a broad distribution between 106° and 132°.

C. Amorphous $CdTeO_2$

Figure 9 shows the PDF of $CdTeO_2$ and the contributions of the partial PDFs $[c_i c_j g_{ij}(r)]$. The first and second coordination shells display average bond lengths of 1.98 Å (Te-O bonds) and 2.23 Å (Cd-O bonds). The following peak at 2.88 Å has a contribution from Cd-Te bonds. However, the major contribution at 2.88 Å is from O-O distances in O-Cd-O and O-Te-O angles (see also Figs. 10 and 12). The other peaks in the PDF correspond to geometrical correlations that are too far to be chemical bonds. The function $g_{\text{Te-O}}(r)$ has a shoulder at 2.18 Å. Like in CdTeO, this shoulder is related to tellurium-axial-oxygen bonds in bipyramids that are TeO_2-like.

Figure 10 shows the atomic environments. This is less diverse than for CdTeO, indicating some greater short-range order. Cd is found coordinated by six O atoms forming a distorted octahedron [cluster (1)], and in other configurations [clusters (2)–(5)] that are obtained from O octahedron by eliminating some O atoms, and replacing other O atoms by

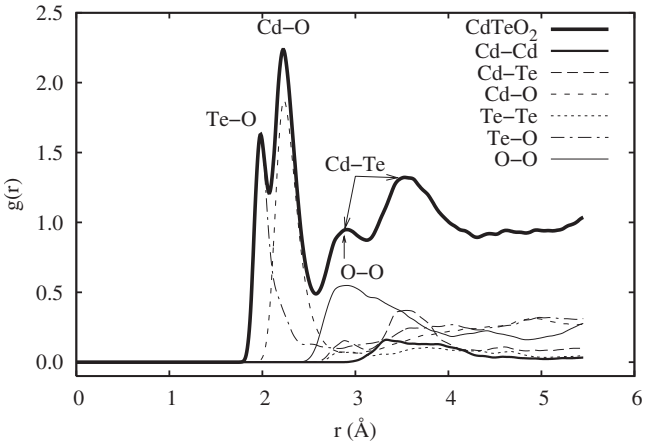

FIG. 9. Total and partial pair distribution functions of a-$CdTeO_2$.

Te atoms. Cd may also have a Cd neighbor at 3.17 Å, as in cluster (8). Te environments are more diverse. There appears a distorted tetrahedron [cluster (6)] with Cd and Te at the vertices; there is a pyramid with Cd and Te at the vertices and Te at the center [cluster (7)], TeO_2-like trigonal bipyramids [cluster (11)], trigonal pyramids with O atoms at the base [cluster (12)], and variations in this trigonal pyramid with three Cd at the base [cluster (10)], and with Cd, Te, and O at the base [cluster (9)]. There is a quasiplanar Te_3O_2 cluster (13), and a Te_2O_3Cd cluster (14), where the O and Te atoms are in the same plane. O environments are in the bottom row of Fig. 10. OCdTe [cluster (15)], $OCdTe_2$ [cluster (16)], and OCd_2Te [cluster (17)] clusters are quasiplanar, and OCd_4 [cluster (18)] forms a distorted tetrahedron. None of these clusters is appreciated as predominant.

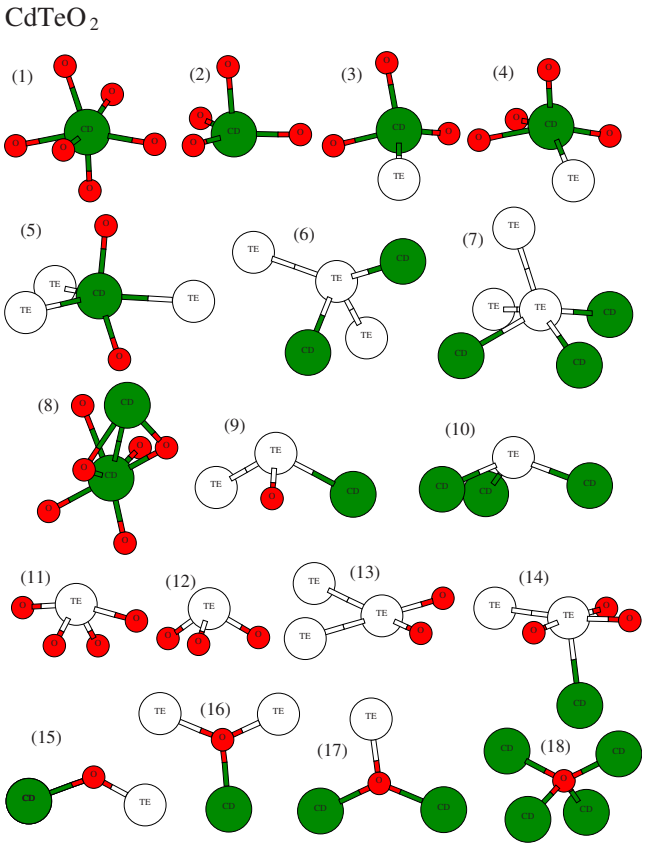

FIG. 10. (Color online) Typical atomic environments in a-$CdTeO_2$. Filled big spheres, empty spheres, and small spheres correspond to Cd, Te, and O atoms, respectively.

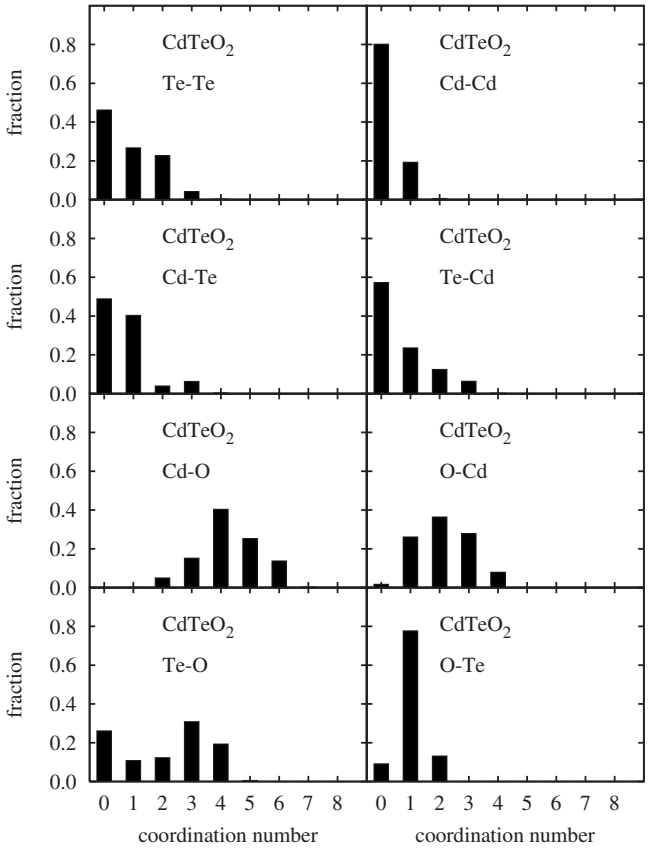

FIG. 11. Histogram of the distribution of the coordination numbers in a-$CdTeO_2$. The cutoff radii are the same as in Fig. 3.

On average, Cd atoms are surrounded by 4.3 O atoms and 0.69 Te atom. Te atoms are surrounded by 2.1 O atoms and 0.69 Cd atom. O atoms are surrounded by 2.1 Cd atoms and 1.0 Te atom. A histogram of the distribution of the Cd-O and Te-O coordination numbers is given in Fig. 11. Cd atoms are mainly coordinated by three to six O atoms (in fractions of 15%, 40%, 25%, and 14%), and either one (40%) or none (49%) Te atom. Te atoms are coordinated by one to four O atoms (11%, 12%, 31%, and 19%), one or two Cd atoms (24% and 12%). O atoms are coordinated by one (78%) or two (13%) Te, and one to three Cd atoms (26%, 36%, and 28%). Nearly 49% of Cd atoms are not linked to Te atoms, 57% of Te atoms are not linked to Cd atoms, and 26% of Te atoms are not linked to O atoms.

The ADFs of the Cd-O and Te-O bonds are shown in Fig. 12(a). The most probable angles are O-Cd-O and Cd-O-Te, with maxima at 88° and 105°. Following in importance are the angles O-Te-O, Cd-O-Cd, and Te-Cd-O [Fig. 12(b)], all of which have maxima between 80° and 100°. The Cd-O-Cd has another maximum at 128°, as in clusters (17) and (18) of Fig. 10.

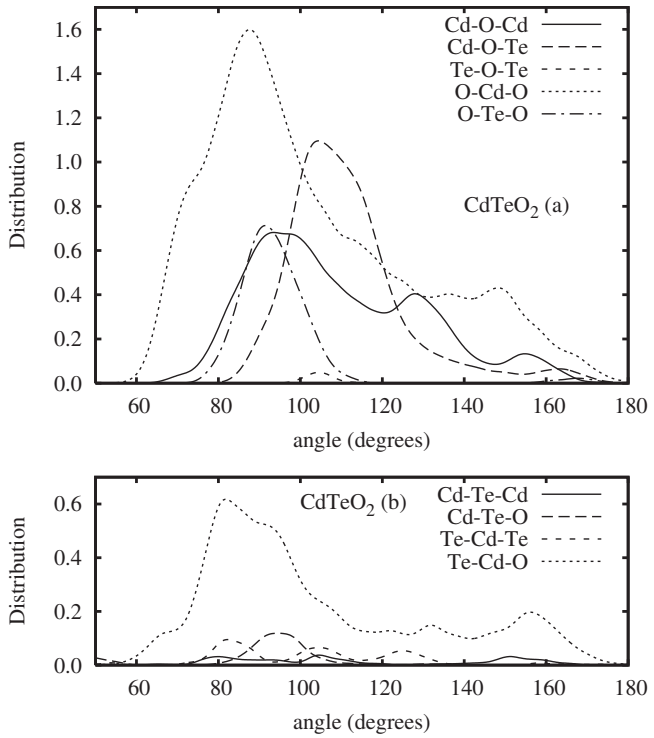

FIG. 12. Angle distribution functions for a-$CdTeO_2$. In part (a) are the angles involving Te-O and Cd-O bonds. In part (b) are the angles involving Cd-Te and Te-Te bonds.

D. Amorphous $CdTeO_3$

Figure 13 shows the PDF of a-$CdTeO_3$ and the contributions of the partial PDFs. The first and second coordination shells display average bond lengths of 1.97 Å (Te-O bonds) and 2.25 Å (Cd-O bonds). The function $g_{\text{Te-O}}(r)$ has a secondary maximum at 2.36 Å, which is too far to constitute a chemical bond (see below). The other peaks in the PDF correspond to geometrical correlations that are too far to be chemical bonds.

Figure 14 shows the atomic environments. It shows less diversity than previous compositions. Cd is coordinated by either six [cluster (1)] or five [cluster (2)] O atoms. Cd may

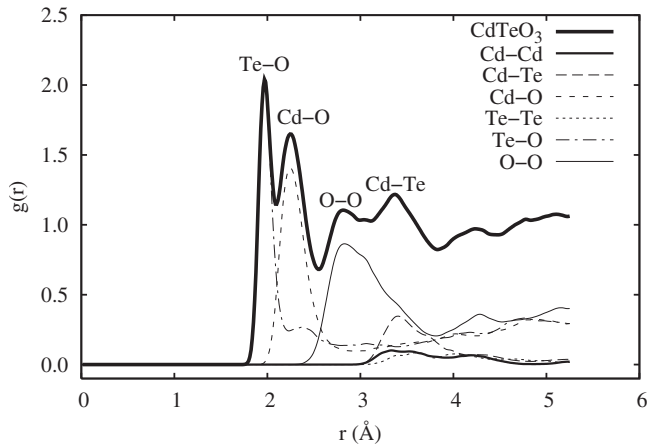

FIG. 13. Total and partial pair distribution functions of $CdTeO_3$.

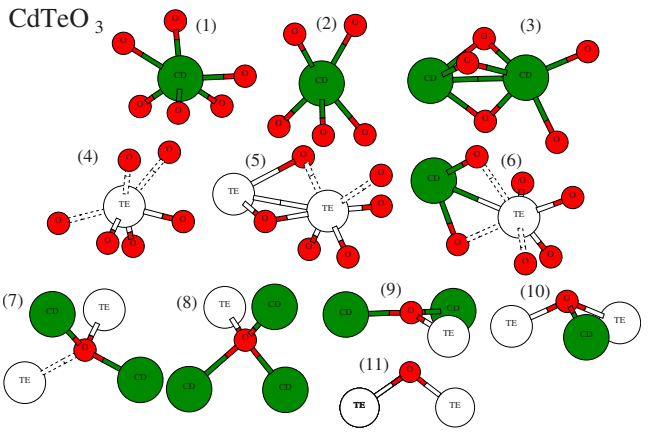

FIG. 14. (Color online) Typical atomic environments in $CdTeO_3$. Filled big spheres, empty spheres, and small spheres correspond to Cd, Te, and O atoms, respectively.

also have a Cd neighbor within the cutoff distance of 3.19 Å, as in cluster (3), similar to the case of $CdTeO_2$. Te atoms are located at the apices of trigonal pyramids [clusters (4) and (6)] or bipyramids [cluster (5)], such as in crystalline TeO_2 and $CdTeO_3$. Other nearest neighbors are indicated in the figure, using dashed lines to indicate distances larger than the cutoff radii of 2.32 Å. This situation looks similar to the case of α-TeO_2, where only four of the six neighbors of Te atoms are chemically bound to Te.[29] Here, in amorphous $CdTeO_3$, there are some TeO_4 bipyramids with symmetric equatorial bonds, and other bipyramids that have one very long bond and three smaller bonds, indicating that a TeO_3 trigonal pyramid is the chemical unit. This basic unit may also have a Cd or Te neighbor within the cutoff distance of 3.19 Å, as in clusters (5) and (6). O atoms can be found in tetrahedral environments, coordinated by one Te and three Cd [cluster (8)], or two Te and two Cd [cluster (7)]. O is also found to be three-coordinated by one (or two) Te and two (or one) Cd, as in clusters (9) and (10). Finally, there is a small fraction of O atoms without Cd neighbors, bound to two Te atoms (11). The most frequent clusters are CdO_6, CdO_5, TeO_3, and TeO_4.

The average coordination numbers were computed using the same radii as for the other compositions (2.32 Å for Te-O). On average, Cd atoms are surrounded by 5.7 O atoms, Te atoms are surrounded by 3.4 O atoms, and O atoms are surrounded by 1.9 Cd atoms and 1.1 Te atom. A histogram of the distribution of the Cd-O and Te-O coordination numbers is given in Fig. 15. Cd atoms are mainly coordinated by five (32%) or six (61%) O atoms, Te atoms are coordinated by three (60%) and four (38%) O atoms. O atoms are coordinated by one (82%) or two (16%) Te atom and one to three Cd atoms (26%, 45%, and 21%). There is a residual fraction of O atoms that are not connected to either Cd or Te.

The ADFs of the Cd-O and Te-O bonds are shown in Fig. 16. These were computed using cutoff radius of 2.20 Å for Te-O bonds, which is the minimum of the partial PDF $g_{\text{Te-O}}(r)$. The most frequent angle is O-Cd-O, its ADF has maxima at 73.5° and 89.5°, and 138°. The O-Te-O ADF has only one maximum at 87°. The rest of the ADFs have one or two maxima and long tails at high angles: Cd-O-Cd has

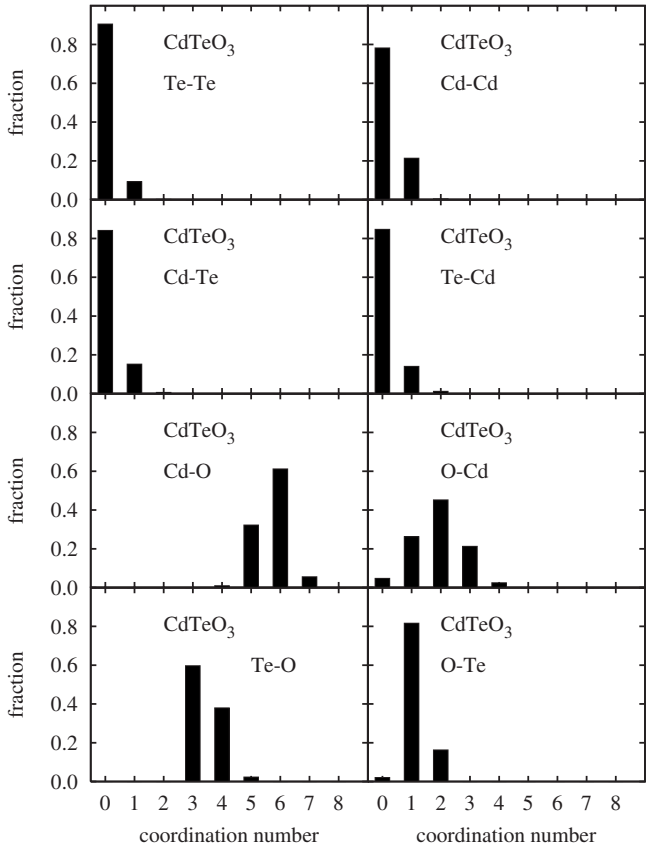

FIG. 15. Histogram of the distribution of the Cd-O and Te-O coordination numbers in $CdTeO_3$. The cutoff radii are the same as in Fig. 3.

maximal probability at 89° and 130°, and Cd-O-Te has one at 101°. Te-O-Te angles have low probability because most oxygen atoms link to only one Te atom.

IV. DISCUSSION

Figure 17 shows the PDF for all the compounds. The heights of Te-O, Cd-O, and Cd-Te peaks change monotonically with the composition. The transition between CdTe-like PDF to $CdTeO_3$-like PDF seems to be near $CdTeO_{0.2}$. However, even for such a low O content, Te-O and Cd-O bonds are well defined.

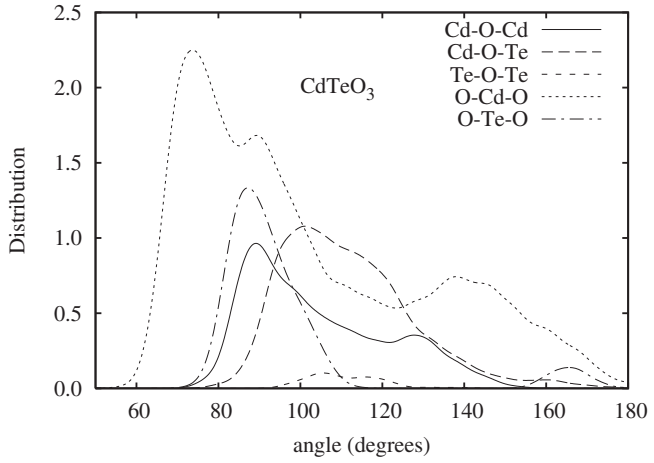

FIG. 16. Bond-angle distributions in $CdTeO_3$. Only Cd-O and Te-O bonds are considered.

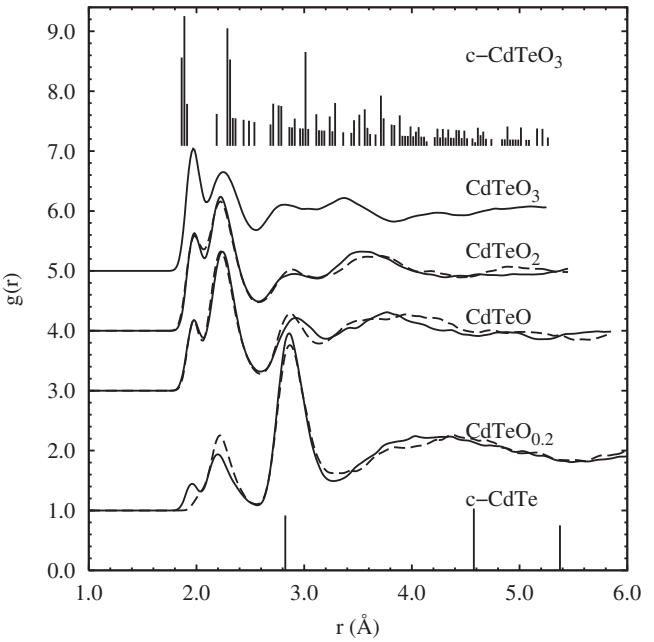

FIG. 17. Total and partial pair distribution functions of amorphous CdTeO, $CdTeO_2$, and $CdTeO_3$. Also are indicated the pair-correlation distances for crystalline CdTe and $CdTeO_3$. For CdTeO and $CdTeO_2$, PDFs of alternative simulations are indicated in dashed lines (see the Appendix).

$CdTeO_{0.2}$ is well differentiated from the other compositions with respect to CdTe-like structures. It is the only composition for which the Cd-Te bonds dominate the PDF and the ADF, while showing the emergence of Cd-O and Te-O bonds. The Cd-Te peak at 2.86 Å compares well to the 2.82 Å distance in crystalline CdTe. The difference of 1.4% of the bond length is probably due to the trend of overestimating the length scales in GGA calculations. However, the examination of the atomic environments in $CdTeO_{0.2}$, as well as the numerical analysis, reveals strong distortion of CdTe-like structural units. One signature of this distortion is the Cd-Te-Cd ADF, which has maximum at 90°, instead of the value of 109.5° of crystalline CdTe.

Figure 18 displays the coordination number distributions for all the compositions in a comparative perspective. The coordination number distributions are qualitatively different for $CdTeO_{0.2}$ on the one side, and for $CdTeO_2$ and $CdTeO_3$ on the other side. The CdTeO distributions have mixed features, being like $CdTeO_{0.2}$ for some pairs (Cd-Te and Te-O) and like $CdTeO_2$ and $CdTeO_3$ for other pairs (Te-Cd and Cd-O). The general trends that can be appreciated are the following. First, the Te-Te and Cd-Cd distributions have maxima for zero neighbors, except in CdTeO which have a weak maximum at one, and decay rapidly with the number of neighbors. Te-Te and Cd-Cd bonds seem to appear as consequence of the frustration induced by the lack of stoichiometry. The fact that the decay is slower for CdTeO and $CdTeO_2$ may be explained by $CdTeO_{0.2}$ and $CdTeO_3$ being

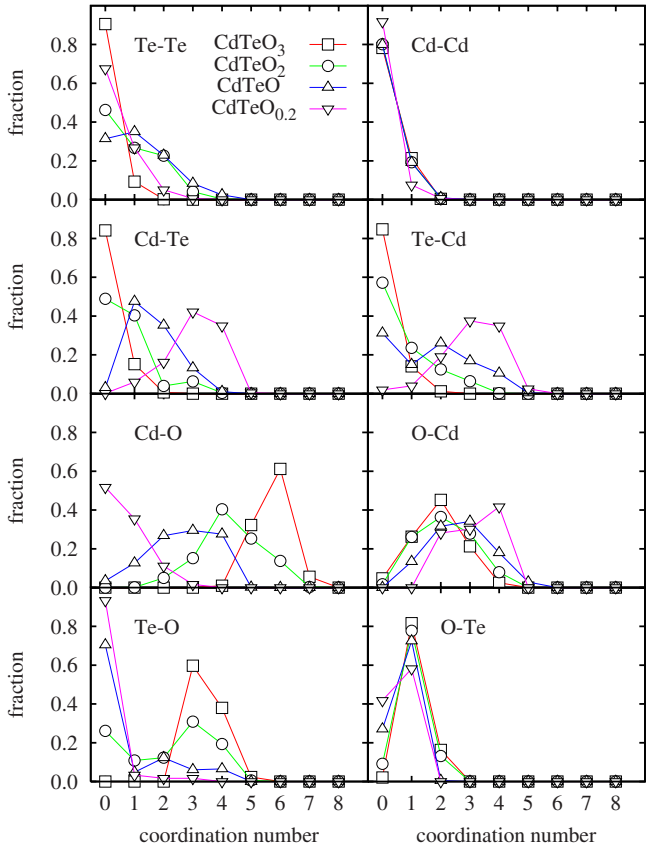

FIG. 18. (Color online) Distribution of the coordination numbers in a-$CdTeO_x$ computed with cutoff radii of 3.19 Å for Cd-Te and Cd-Cd, 3.27 Å for Te-Te, 2.90 Å for Cd-O, and 2.32 Å for Te-O.

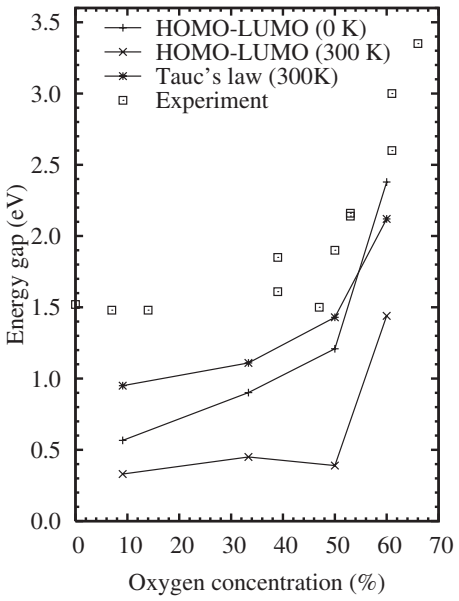

FIG. 19. Comparison of the experimental and theoretical band gaps. The experimental values are from Ref. 9.

closer to stoichiometry. Second, the O-Te distribution (Te around O) has the maximum fraction at one for all the compositions. Third, the Cd-Te coordination (Te around Cd) in $CdTeO_{0.2}$ and CdTeO has zero fraction for zero neighbors and maxima at tree and one, respectively, while in the other compositions, the distribution is maximal at zero neighbors and decays rapidly. However, the Te-Cd (Cd around Te) distribution places CdTeO in the group of $CdTeO_2$ and $CdTeO_3$, with nonzero fraction for zero neighbors.

The typical atomic environments are found in crystalline CdTe, CdO, TeO_2, and $CdTeO_3$. However, there are also others that are not present in the crystalline phases. Conversely, there are structures which are not present in the amorphous compounds. For example, TeO_6 octahedra, common to some crystalline Cd-Te-O compounds,[28,29] are not present in the obtained structures. Only in $CdTeO_3$ we find clusters with Te atoms surrounded by six O atoms, but analyzing the Te-O distances, we estimate that only three or four O atoms are effectively bound to the central Te, thus forming the trigonal pyramids of crystalline $CdTeO_3$ or the bipyramids of TeO_2. Interestingly, $CdTeO_3$ has the most ordered environment of all the $CdTeO_x$ compounds: most Te atoms are tricoordinated, Cd has coordinations of 5 and 6, such as in the crystalline phase. CdTeO and $CdTeO_2$ display less short-range order, the coordination numbers of Te and Cd presenting greater variability. The net coordination numbers follow the expected variation between the limits of CdTe and $CdTeO_3$.

In $CdTeO_{0.2}$, the most abundant clusters are $TeCd_4$, $CdTe_4$, $TeCd_3$, $CdTe_3O$. In $CdTeO_3$, the most abundant clusters are CdO_6, CdO_5, TeO_3, and TeO_4.

CdTeO and $CdTeO_2$ present no predominant type of cluster. The chemical disorder is greater for these compounds with intermediate O content. In particular, in CdTeO, O and Te atoms can occupy the same sites in the structural units. Moreover, for this compound the probability of finding Cd-Cd and Te-Te bonds is maximal. As only CdTe and $CdTeO_3$ are stoichiometric, it seems that departure from stoichiometry increase the chemical and topological disorder.

Our results provide arguments against the statistical model of Ref. 15 where it was postulated that the basic units are CdTe and polymers of TeO_4 units completed by Cd atoms that satisfy locally the valence rules. Although we have not attempted to identify clusters that satisfy the valence rules, it is clear that the TeO_4 units cannot be regarded as basic building units of a-$CdTeO_x$. A recent paper[22] reported Raman measurements on Cd-Te-O thin films and interpreted them based on similarities with crystalline CdO and γ-TeO_2 and with telluritic glasses. This interpretation assigns a fundamental role to vibrational modes of TeO_3 and TeO_4 units, as well as to Cd-O bond stretching. The structural models obtained in this work contain all these types of clusters, providing the basis for a phonon calculation that allows a direct comparison with the Raman spectra.

It is interesting to compare the band gap of our structural models with the experimental values.[9] This comparison is shown in Fig. 19. The gap E_G has been obtained by fitting the absorption coefficient α with the Tauc's law $(h\nu\alpha)^{1/2} = A(h\nu - E_G)$. For the theoretical values, we estimate α as proportional to the joint density of states (JDOS), which is obtained from the Kohn-Sham energies of all the configurations of the ensemble. We also plot the highest occupied

TABLE I. Coordination numbers. n_{i-j} is the average number of atoms of type j around an atom of type i within a cutoff distance R_{i-j}. For CdTeO and $CdTeO_2$, the values enclosed in brackets correspond to alternative samples, as described in the text.

		n_{i-j}			
$i-j$	R_{i-j}	$CdTeO_{0.2}$	CdTeO	$CdTeO_2$	$CdTeO_3$
Te-O	2.32	0.1 (0.1)	0.7 (0.8)	2.1 (2.2)	3.4
O-Te	2.32	0.7 (0.5)	0.7 (0.8)	1.0 (1.1)	1.1
Cd-O	2.90	0.6 (0.7)	2.7 (2.6)	4.3 (4.1)	5.7
O-Cd	2.90	2.8 (3.4)	2.7 (2.6)	2.1 (2.1)	1.9
Cd-Te	3.19	3.1 (3.0)	1.6 (1.6)	0.7 (0.8)	0.2
Te-Cd	3.19	3.1 (3.0)	1.6 (1.6)	0.7 (0.8)	0.2
Te-Te	3.27	0.3 (0.5)	1.2 (0.9)	0.9 (0.7)	0.1

molecular orbital (HOMO)–lowest unoccupied molecular orbital (LUMO) gaps of the ensemble (300 K) and of the relaxed configuration (0 K). All the gap estimates reproduce roughly the experimental tendency. This provides support to the structural models that we have generated.

In summary, we have obtained structural models for the amorphous materials a-$CdTeO_{0.2}$, a-CdTeO, a-$CdTeO_2$, and a-$CdTeO_3$, using *ab initio* molecular dynamics. We have made a detailed description of the variety of atomic environments found in these materials, and we have characterized them using statistical functions, such as the partial distribution functions, the angle distribution functions, and the coordination number histograms. We have found that a-CdTeO and a-$CdTeO_2$ present more chemical and topological disorder than a-$CdTeO_{0.2}$ and a-$CdTeO_3$.

ACKNOWLEDGMENTS

This work was supported by FONDECYT (Chile) Grants No. 1050293 and No. 7060248 and PBCT (Chile) Grant No. ACT/24. We thank S. Scandolo for useful advice. We also acknowledge grants of computer time from DEMOCRITOS, the Abdus Salam International Centre for Theoretical Physics, and the Center of Bioinformatics and Molecular Simulation of the University of Talca. V. Bernales is acknowledged for help with the cluster pictures. This work was motivated by J. L. Peña of the Centro de Investigación y Estudios Avanzados del Instituto Politécnico Nacional of Mexico some 10 years ago.

APPENDIX: ALTERNATIVE SAMPLES

A few words must be said about the robustness of these simulations. We attempted to determine the densities of the different compounds using variable cell damped molecular dynamics, starting from a configuration equilibrated at 3000 K. This method works for CdTe, obtaining a density almost equal to value obtained minimizing the energy of the perfect crystal. However, for $CdTeO_3$, the density obtained from damped variable cell MD was 15% smaller than the value obtained relaxing the crystalline structure. This result only confirms that the ternary compound is more difficult to relax, as could be expected due to its complex structure. On the other hand, keeping the cell volume and shape fixed and using different thermalization strategies, we obtained configurations of a-$CdTeO_3$ with very similar energies at 300 K. In addition to the method described in Sec. II, we also generated structures as follows. We made successive cycles of velocity rescaling and constant energy MD at 3000, 1300, 800, and finally 300 K. One simulation was made in a supercell of constant volume corresponding to the physical density, while the other was made in a supercell with enlarged volume, and at 300 K the supercell was rescaled to the physical density. It turns out that the three configurations obtained at 300 K differ in total energy by less than 10 meV/atom, with the smallest energy obtained with the general method adopted in this work. This suggests that the structure of $CdTeO_3$ that we obtain is rather robust.

For $CdTeO_{0.2}$ we searched additional ensembles in order to improve the statistics of oxygen environments, as the simulation cell has only six atoms. The last configuration of the first ensemble was reheated to 3000 K and annealed again to 300 K. As a result, we obtained an ensemble with practically the same energy, but corresponding to a different energy valley of the phase space. The ensembles have some differences in the statistical descriptors, specially those related to oxygen. The figures of Sec. III A correspond to the average of both ensembles. However, in Fig. 17 both PDFs are shown separately to provide an estimation of the statistical errors. The coordination numbers of this ensemble are shown in parentheses in Table I. We obtained a third ensemble, doing the annealing from 3000 to 2000 K for 1 ps, then from 2000 to 1000 K, and from 1000 to 300 K. The energy of this ensemble was 21 meV/atom higher than for the first and second ensembles, and was not considered in for the averaged statistical properties. However, the properties of this ensemble are quite similar to those of the first and second ensembles.

For CdTeO, we also show the PDF for an alternate sample, corresponding to a different energy valley of the phase space. We made an alternative simulation, running more time at 3000 K, before doing the Berendsen rescaling to 300 K. This produced a structure 1 meV/atom less in total energy; hence both configurations are almost equally probable. The analyses of the PDF, ADF, and coordination num-

bers are very similar. The coordination numbers of these alternate samples are shown enclosed in brackets in Table I.

We analyzed two samples of the $CdTeO_2$. One of them (sample I) was prepared by the standard method. However, we obtained another configuration (sample II) that has an average potential energy 10 meV/atom lower than the first one. This configuration was obtained by a different annealing sequence, in which the Berendsen thermostat was mistakenly applied during 2.5 ps with a relaxation time $\tau=500$ fs (instead of 1000 fs). The simulation was then stopped (instantaneous temperature was 327 K) and restarted with zero velocities, during 5 ps with $\tau=200$ fs, and finally with $\tau=400$ fs such as in our standard procedure. The result is that despite having performed a faster cooling than in the standard procedure, the system fell in a local valley of smaller energy. This shows that using the slowest possible cooling rate does not warrant to obtain the configuration of minimal energy. The results reported correspond to the structure of minimal average energy (sample II). In Fig. 17 we show the PDF for both samples. In Table I the coordination numbers of sample I are listed enclosed in brackets. Both structures are similar in coordination numbers and PDF, only differing in some of the angle distribution functions. However, the differing ADF correspond to bonds present in small fractions, thus being more sensitive to statistical errors.

[1] K. Zanio, in *Cadmium Telluride*, Semiconductors and Semimetals Vol. 14, edited by P. K. Willardson and A. C. Beer (Academic, New York, 1978).
[2] M. A. Green, K. Emery, Y. Hisikawa, and W. Warta, Prog. Photovoltaics **15**, 425 (2007).
[3] A. Ebina, K. Asano, and T. Takahashi, Phys. Rev. B **22**, 1980 (1980).
[4] G. D. Davis, T. S. Sun, S. P. Buchner, and N. E. Byer, J. Vac. Sci. Technol. **19**, 472 (1981).
[5] F. Wang, A. Schwartzman, A. L. Fahrenbruch, R. Sinclair, R. H. Bube, and C. M. Stahle, J. Appl. Phys. **62**, 1469 (1987).
[6] S. S. Choi and G. Lucovsky, J. Vac. Sci. Technol. B **6**, 1198 (1988).
[7] Z. K. Heiba, Cryst. Res. Technol. **38**, 488 (2003).
[8] R. Miotto, F. D. Kiss, and A. C. Ferraz, Surf. Sci. **525**, 24 (2003).
[9] F. J. Espinoza-Beltrán, O. Zelaya, F. Sánchez-Sinencio, J. G. Mendoza-Álvarez, M. H. Farias, and L. Baños, J. Vac. Sci. Technol. A **11**, 3062 (1993).
[10] A. Zapata-Navarro, M. Zapata-Torres, V. Sosa, P. Bartolo-Pérez, and J. L. Peña, J. Vac. Sci. Technol. A **12**, 714 (1994).
[11] A. Zapata-Navarro, P. Bartolo-Pérez, M. Zapata-Torres, R. Castro-Rodríguez, and J. L. Peña, J. Vac. Sci. Technol. A **15**, 2537 (1997).
[12] M. Y. El Azhari, M. Azizan, A. Benouna, A. Outzourhit, E. Ameziane, and M. Brunel, Thin Solid Films **295**, 131 (1997).
[13] M. Y. El Azhari, M. Azizan, A. Bennouna, A. Outzourhit, E. Ameziane, and M. Brunel, Thin Solid Films **366**, 82 (2000).
[14] P. Bartolo-Pérez, J. L. Peña, and M. H. Farias, Superficies y Vacio **8**, 59 (1999).
[15] A. Iribarren, E. Menéndez-Proupin, F. Caballero-Briones, R. Castro-Rodriguez, and J. L. Peña, J. Appl. Phys. **86**, 4688 (1999).
[16] F. Caballero-Briones, A. Zapata-Navarro, P. Bartolo-Pérez, R. C. Rodríguez, M. Zapata-Torres, W. Cauich, and J. L. Peña, Rev. Mex. Fis. **44** S3, 268 (1998).
[17] H. Arizpe-Chávez, R. Ramírez-Bon, F. Espinoza-Beltrán, O. Zelaya-Angel, J. Marín, and R. Riera, J. Phys. Chem. Solids **61**, 511 (2000).
[18] A. Iribarren, E. Menéndez-Proupin, F. Caballero-Briones, R. Castro-Rodriguez, and J. L. Peña, Mod. Phys. Lett. B **15**, 643 (2001).
[19] P. Bartolo-Pérez, R. C. Rodríguez, F. Caballero-Briones, W. Cauich, J. L. Peña, and M. H. Farias, Surf. Coat. Technol. **155**, 16 (2002).
[20] R. Castro-Rodríguez, A. Iribarren, P. Bartolo-Pérez, and J. L. Peña, Thin Solid Films **484**, 100 (2005).
[21] F. Caballero-Briones, A. I. Oliva, P. Bartolo-Pérez, A. Zapata-Navarro, and J. L. Peña, Thin Solid Films **516**, 8289 (2008).
[22] F. Caballero-Briones, J. L. Peña, A. Martel, A. Iribarren, O. Calzadilla, S. Jiménez-Sandoval, and A. Zapata-Navarro, J. Non-Cryst. Solids **354**, 3756 (2008).
[23] J. Carmona-Rodríguez, R. Lozada-Morales, O. Jiménez-Sandoval, F. Rodríguez-Melgarejo, M. Meléndez-Lira, and S. J. Jiménez-Sandoval, J. Appl. Phys. **103**, 123516 (2008).
[24] R. Castro-Rodríguez, J. L. Peña, F. Leccabue, B. E. Watts, and E. Melioli, Appl. Phys. Lett. **87**, 061916 (2005).
[25] Y. J. Shan, K. Sasaki, K. Sudo, H. Imoto, and M. Itoh, Jpn. J. Appl. Phys., Part 2 **41**, L780 (2002).
[26] H. Tetsuka, Y. J. Shan, K. Tezuka, and H. Imoto, Solid State Commun. **137**, 345 (2006).
[27] V. Krämer and G. Brandt, Acta Crystallogr., Sect. C: Cryst. Struct. Commun. **41**, 1152 (1985).
[28] M. Weil, Solid State Sci. **6**, 29 (2004).
[29] E. Menéndez-Proupin, G. Gutiérrez, E. Palmero, and J. L. Peña, Phys. Rev. B **70**, 035112 (2004).
[30] F. Pietrucci, S. Caravati, and M. Bernasconi, Phys. Rev. B **78**, 064203 (2008).
[31] D. Marx and J. Hutter, in *Modern Methods and Algorithms of Quantum Chemistry*, NIC Series Vol. 3, edited by J. Grotendorst (Forschungszentrum Jülich, 2000), pp. 301–409.
[32] J. Sarnthein, A. Pasquarello, and R. Car, Phys. Rev. Lett. **74**, 4682 (1995).
[33] V. V. Godlevsky, M. Jain, J. J. Derby, and J. R. Chelikowsky, Phys. Rev. B **60**, 8640 (1999).
[34] E. Ko, M. M. G. Alemany, J. J. Derby, and J. R. Chelikowsky, J. Chem. Phys. **123**, 084508 (2005).
[35] See EPAPS Document No. E-PRBMDO-78-102845 for the atomic coordinates in XYZ format. For more information on EPAPS, see http://www.aip.org/pubservs/epaps.html.
[36] E. Menéndez-Proupin, G. Gutiérrez, E. Palmero, and J. L. Peña, Phys. Status Solidi C **1**, S104 (2004).
[37] T. Ushino and T. Yoko, J. Non-Cryst. Solids **204**, 243 (1996).
[38] T. Sekiya, N. Mochida, A. Oshtsuka, and M. Tonokawa, J. Non-

Cryst. Solids **144**, 128 (1992).
[39] M. P. Allen and D. J. Tildesley, *Computer Simulation of Liquids*, 1st ed. (Oxford University Press, Bristol, 1989).
[40] S. Baroni, A. D. Corso, S. de Gironcoli, P. Giannozzi, C. Cavazzoni, G. Ballabio, S. Scandolo, G. Chiarotti, P. Focher, A. Pasquarello, K. Laasonen, A. Trave, R. Car, N. Marzari, and A. Kokalj, QUANTUM-ESPRESSO package, 2005 (http://www.quantum-espresso.org/).
[41] J. P. Perdew, K. Burke, and M. Ernzerhof, Phys. Rev. Lett. **77**, 3865 (1996).
[42] Cd.pbe-n-van.UPF and O.pbe-rrkjus.UPF from the QUANTUM-ESPRESSO distribution.
[43] Te.pbe-rrkj.UPF in the QUANTUM-ESPRESSO distribution.
[44] D. Vanderbilt, Phys. Rev. B **41**, 7892 (1990).
[45] A. M. Rappe, K. M. Rabe, E. Kaxiras, and J. D. Joannopoulos, Phys. Rev. B **41**, 1227 (1990).
[46] N. E. Cusack, *The Physics of Structurally Disordered Matter: An Introduction*, Graduate Student Series in Physics (Institute of Physics, Bristol, 1987).
[47] File Utilities for Molecular Dynamics, http://www.gnm.cl/software/fumody